INTERPRETATION OF SINGLE-DOPPLER RADAR SIGNATURES IN A V-SHAPED HAILSTORM: PART II – EVOLUTION OF UPDRAFT INTERACTIONS WITH AMBIENT MID-ALTITUDE FLOW

Rodger A. Brown

NOAA/National Severe Storms Laboratory
Norman, Oklahoma

Kathleen L. Torgerson

NOAA/National Weather Service Weather Forecast Office
Pueblo, Colorado

Abstract

Part II of this two-part descriptive study documents characteristics and evolution of the mid-altitude flow field arising from interactions of ambient flow with the updraft region of a North Dakota multicell hailstorm. While only single-Doppler radar measurements were available, there were sufficient details in reflectivity and Doppler velocity features to provide interesting deductions about the interactions. The updraft region, located at the upstream end of the storm, typically consisted of two or three actively growing updrafts. Maximum horizontal wind speeds occurred along the lateral flanks of the updraft region. The center of the resulting wake region was characterized by a mid-altitude channel of low-speed air extending downstream from the middle of the updraft region. Characteristics of the resultant mid-altitude vorticity couplet straddling the updraft region did not appear to support the theoretical concept that couplets arise from vertical tilting of low-altitude horizontal vortex tubes. Rather, the vertical momentum of individual updrafts appeared to have collectively presented enough resistance to the approaching mid-altitude environmental flow that air slowed down as it flowed through the porous updraft region. As air farther upstream approached the wall of slower-moving air, some of the air was diverted, increasing speed as it flowed around the sides of the updraft region.

1. Introduction

With establishment of the network of Weather Surveillance Radar-1988 Dopplers (WSR-88Ds) across the United States during the early and mid 1990s, NOAA/National Weather Service (NWS) forecasters and other users of the radars became aware of an interesting Doppler velocity feature that is found at mid-altitudes in some severe thunderstorms. This feature consists of a band of weak Doppler velocity values extending downstream from the high-reflectivity updraft region of the storm. Doppler velocity values stronger than environmental winds are found on the storm's lateral flanks. This wake flow feature is most obvious when mid-altitude environmental flow has a major component toward or away from the radar. Idealized Doppler velocity patterns from several different viewing directions have been simulated by Brown and Wood (1991). The overall single-Doppler velocity pattern resembles that which would be produced by blocked flow (e.g., Kraus 1970; Brown and Crawford 1972).

Prior to widespread use of Doppler radar, perturbation of the mid-altitude flow field by a storm was detected using proximity aircraft measurements (e.g., Shmeter 1966; Fujita and Grandoso 1968; Fankhauser 1971; Browning and Foote 1976; Ramond 1978; Krauss and Marwitz 1984), and by following chaff through and around a storm using conventional radar (e.g., Fankhauser 1971; Jessup 1972). Aircraft measurements reveal the presence of high-pressure perturbations on the upstream edge of strong updrafts (e.g., Ramond 1978). The measured flow field indicates that upstream air decelerates as it encounters the high-pressure region, is diverted, and increases speed as it moves around the lateral flanks of the updraft. At times, flow around the right side of the storm has been observed to be considerably stronger than flow around the left side (e.g., Fujita and Grandoso 1968; Krauss and Marwitz 1984). Right and left sides of a storm refer to the sides seen by an observer located behind the storm and looking in the downstream direction. The updraft region, which typically presents a 10-15 km wide porous obstruction to ambient flow, can produce a wake region that extends downstream for 100 km (e.g., Fujita and Grandoso 1968).

In more recent years, refined measurements from multiple-Doppler radar studies of severe thunderstorms provide more detailed information about the relationship between updrafts and the wake flow field (e.g., Eagleman and Lin 1977; Heymsfield 1978; Knupp and Cotton 1982; Foote and Frank 1983; Miller et al. 1983; Brown 1989; Bluestein and Woodall 1990; Miller et al. 1990; Fankhauser et al. 1992; Reinking and Meitín 1993; Kennedy and Rutledge 1995). At mid-altitudes, the strongest horizontal shear occurs on the lateral flanks of the storm. The strong shear regions are represented by cyclonic vertical vorticity on the right flank and anticyclonic vertical vorticity on the left flank which is called a *vorticity couplet*. The flow decreases speed as it continues downstream, with some of the air converging into the wake low-pressure region directly downstream of the

updraft region. Based on three-dimensional trajectories derived from dual-Doppler radar measurements, some of the mid-altitude air that converges into the center of the wake region descends in one or more downdraft regions within the wake (e.g., Knupp and Cotton 1982; Brown 1989).

There are two basic hypotheses—empirical and theoretical—concerning the origin of the wake region. Both hypotheses are based on interactions of ambient flow with updrafts. The empirical hypothesis envisions mid- and upper-altitude flow being partially obstructed by the semi-permeable updraft region at the upstream end of a thunderstorm. The updraft region is the actively growing portion of the storm where two or more updrafts are found in various stages of development. Individual updrafts are observed to remain vertical even in the presence of increasing wind speed with height (e.g., Dennis et al. 1970; Brown and Torgerson 2003). It is envisioned that the high-momentum vertical velocities in the updrafts within the updraft region act as a partial blocking mechanism. Since the storm is moving slower than the mid- and upper-altitude flow, much of the approaching air is forced to flow around the outer portions of the updraft region, producing the mid-altitude vorticity couplet.

Proponents of the theoretical hypothesis argue that only solid objects can act as obstacles to the flow. Since updraft-relative winds vary with height and updrafts entrain and detrain air, the obstacle analogy cannot be applied to updrafts (e.g., Rotunno and Klemp 1982; Klemp 1987; Davies-Jones et al. 1994). In order to explain the observed obstacle-like flow, a couple of versions of the theoretical hypothesis have been proposed (e.g., Rotunno 1981; Davies-Jones 1984). Since wind speed increases with height in the boundary layer at the earth's surface, the resulting vertical wind shear produces horizontal vorticity that can be represented conceptually by horizontal vortex lines or vortex tubes. It is proposed that vertical tilting of low-altitude horizontal vorticity is responsible for the vorticity couplet at mid-altitudes in thunderstorms.

Rotunno (1981) uses a simple analytical model to explain the existence of the mid-altitude vorticity couplet. He argues that when a horizontal vortex tube oriented perpendicular to the low-altitude flow (called crosswise vorticity) approaches a storm's updraft, the tube is pulled upward into a vertical position as it encounters the updraft. Rotunno speculates that the vortex tube becomes contorted into the shape of an inverted "U", with the updraft in the middle of the inverted "U". The vertical portion of the vortex tube on the right side of the updraft (looking downstream) represents cyclonic horizontal wind shear (cyclonic vertical vorticity), and the vertical portion of the tube on the left represents anticyclonic horizontal wind shear (anticyclonic vertical vorticity). In this way, the mid-altitude vorticity couplet is proposed to be created.

Davies-Jones (1984) uses a "linear (small amplitude) theory of shallow, inviscid, isentropic convection in a dry, unstably stratified, nonrotating atmosphere" to explain the presence of a vorticity couplet. Since isentropic surfaces are material surfaces, air and vortex lines in this hypothetical environment remain on the same surface as they move. Davies-Jones assumes that there is a hump in otherwise horizontal isentropic surfaces. Air approaching the hump flows up the upstream side and produces an updraft. When air flows down the downstream side of the hump, a downdraft is produced. As an initially horizontal vortex line representing crosswise horizontal vorticity rises up over the hump, it acquires an inverted "U" shape, with cyclonic (anticyclonic) vertical vorticity on the right (left) side. Unlike the Rotunno theory that places the vorticity couplet on the lateral flanks of the updraft, the Davies-Jones theory places the vorticity couplet on the lateral flanks of the isentropic hump midway between the upstream updraft and downstream downdraft.

In Part I (Brown and Torgerson 2003) of this two-part paper, the authors used single-Doppler velocity and reflectivity signatures to deduce evolution of updrafts in the V-shaped Carson, North Dakota multicell hailstorm. They found that the localized maximum reflectivity column associated with the deduced growing updraft portion of an updraft/downdraft cell initially was oriented vertically. As the updraft reached its maximum vertical extent (and thus started to weaken), the reflectivity column began tilting either to the left or to the right. They showed that the updraft (represented by the reflectivity column) was responding to flow around a new, nearby strong updraft. If the older updraft was on the right (left) side of the new one, the reflectivity column associated with the older updraft would tilt and move to the right (left), and after updraft demise, hydrometeors within the cell would descend along the right (left) flank of the storm. With new updrafts at the upwind end of the storm randomly forming to the left or right of existing updrafts, hydrometeors descended almost alternately along each flank, producing a pronounced V-shaped echo pattern.

In this Part II, the character and evolution of the mid-altitude flow field adjacent to and downstream of the updraft region in the Carson storm are described using single-Doppler radar measurements. Though only single-Doppler radar measurements are used, there is sufficient detail in reflectivity and Doppler velocity features to provide interesting deductions about the wake flow area.

2. Data Sources

The Carson, North Dakota, multicell hailstorm occurred on the evening of 11 July 1989 during the North Dakota Thunderstorm Project (NDTP). NDTP was conducted from 12 June through 22 July 1989 in south central North Dakota. Its purpose was to study dynamic and microphysical characteristics of northern Great Plains convective storms (Boe et al. 1992). Among the data collection platforms used in the project were six instrumented aircraft, NOAA/Wave Propagation Laboratory's 5-cm NOAA-C Doppler radar, and the North Dakota rain and hail reporting network. The National Center for Atmospheric Research (NCAR) provided two CLASS rawinsonde systems, two Portable Automated Mesonet (PAM) sites, and CP-3 and CP-4 5-cm Doppler radars. The CP-3 radar was located next to the Bismarck airport, and the CP-4 radar was located 56 km to the northwest of CP-3. The North and South Dakota portions of the National Lightning Detection Network (NLDN) became

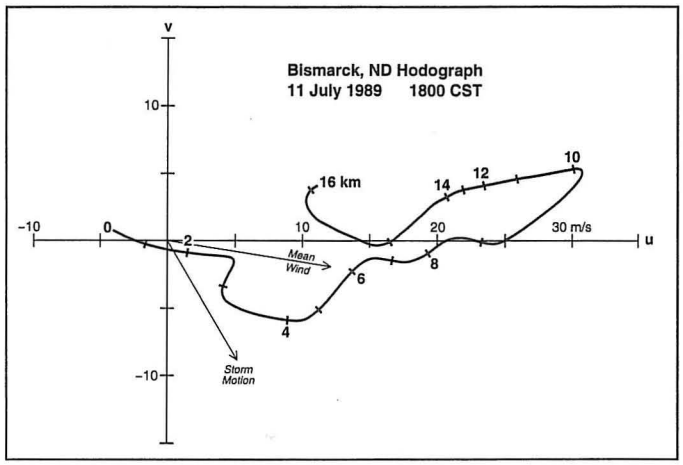

Fig. 1. Hodograph of ground-relative winds measured by the 1800 CST rawinsonde released on 11 July 1989 by the NOAA/National Weather Service in Bismarck, North Dakota. The surface wind was adjusted to agree with observed surface wind at the time. A line was then drawn connecting the surface value with the rawinsonde value at 1 km height. From Brown and Torgerson (2003).

operational in time to use for the project (e.g., Orville 1991). Surface observations and routine 0600 and 1800 CST (all times in this paper are Central Standard Time) rawinsonde releases from the NWS Forecast Office in Bismarck were incorporated into the project data set. GOES-7 visual and infrared satellite data provided an overview of convective storm activity.

Of the two NCAR Doppler radars, only CP-3 was used for this study of the Carson storm; CP-4 started to collect data as the storm was dying. The CP-3 radar completed sectorized scans through the storm in 3–5 minutes, with a new three dimensional scan starting every 4–7 minutes. Twenty-two volume scans were collected between 2152 and 2400 CST. To study storm evolution at consistent heights, CP-3 Doppler velocity and reflectivity data were interpolated to a three dimensional Cartesian grid using the NOAA/National Severe Storms Laboratory's Multiple-Doppler Radar Analysis (RADAN) System (e.g., Brown et al. 1981). Prior to interpolation, radar data within each three dimensional volume were adjusted to a common reference time in order to correct for storm motion (330°, 10.3 m s^{-1}) during the period of data collection. A three-dimensional Cressman (1959) weighting function was used to interpolate polar radar data to a three-dimensional Cartesian grid having 1 km spacing in all three directions. Owing to the inherent smoothing nature of data interpolation, isolated extreme radar reflectivity values typically decreased by 1–6 dBZ as a result of interpolation. Similarly, the magnitude of extreme Doppler velocity values decreased by a few meters per second.

3. The Storm and Its Environment

As discussed in Part I, the Carson storm formed about 2015 CST (prior to Doppler radar data collection) ahead of a squall line that moved south-southeastward across nearly all of North Dakota. Most of the time, the storm

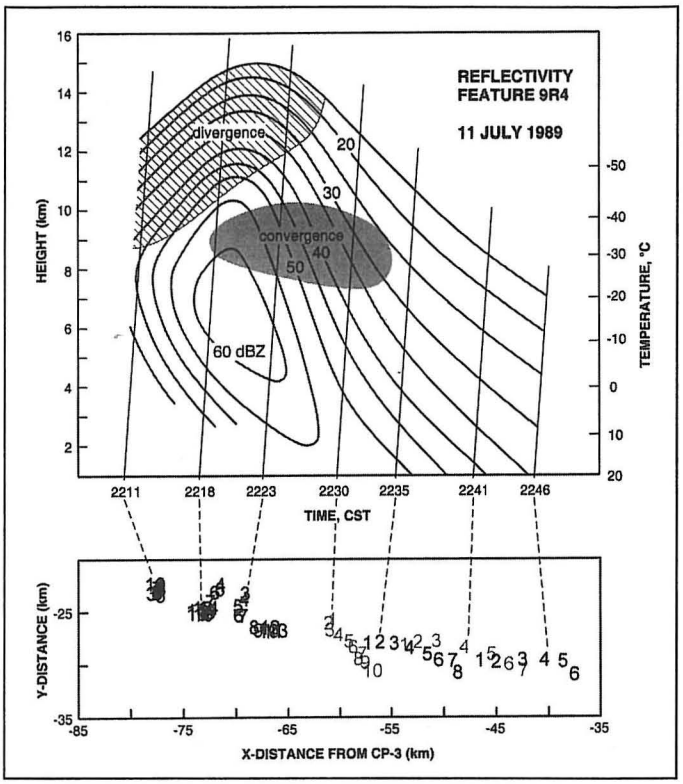

Fig. 2. Four-dimensional depiction of reflectivity feature 9R4. Top portion of figure is a time height plot of the feature; contour interval is 5 dBZ. Each angled vertical line represents data collection as a function of height and time for a given radar volume scan. Maximum reflectivity values were plotted at 1 km height increments and then smoothed contours were drawn. Hatched area indicates times and heights where single Doppler velocity signatures of divergence were detected in upper portions of the updraft. Shaded area indicates times and heights where single-Doppler velocity signatures of convergence were detected in the upper portion of downdraft induced by descending hydrometeors. Bottom portion of figure shows projection of 9R4 data points (1-km intervals) onto a horizontal x,y plane. Location of the number denotes projected location of the feature center; the number represents height in km. Each dashed line connects the reference time of the volume scan above with the corresponding projected data points. Adapted from Brown and Torgerson (2003).

was over sparsely populated areas. However, when the storm passed over the small community of Carson, there were reports of up to baseball sized hail in the general area starting at 2235 CST, and lasting for 15 minutes (NCDC 1989).

The environmental hodograph (Fig. 1) indicates that the mean wind was 12.4 m s^{-1} from 279°, averaged over 50-hPa intervals from the lifting condensation level (800 hPa, 1.6 km above ground) to the equilibrium level (250 hPa, 10.4 km). Mean shear vector over the same depth was 3 x 10^{-3} s^{-1} toward 083°. Individual convective cells within the storm moved generally in the direction of the mean wind. However, overall storm motion was from 330° at 10.3 m s^{-1}, propagating about 50° to the right of the meanwind.

The presence of updraft/downdraft cells in the Carson storm were deduced from reflectivity and Doppler velocity signatures, as discussed in Part I. In plan view, a cell was

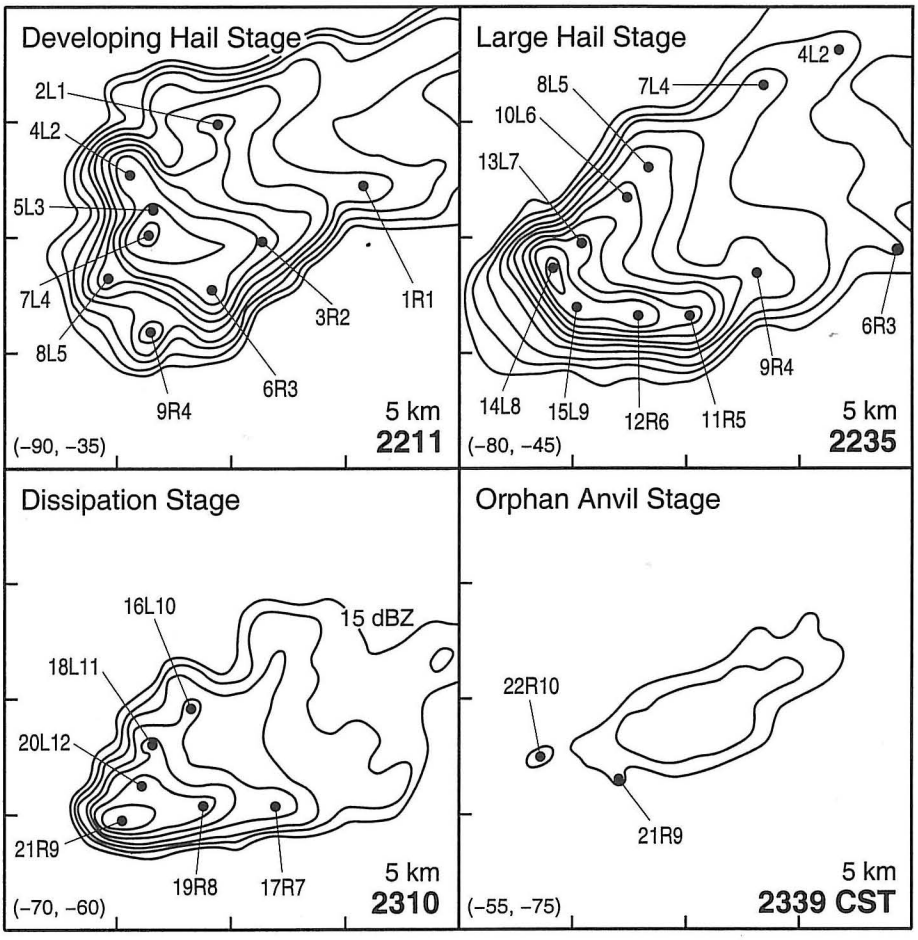

Fig. 3. Sample of horizontal reflectivity fields at 5 km height during four stages of development in the Carson storm. Reflectivity contours are at 5 dBZ intervals beginning with 15 dBZ. Dots indicate centers of labeled reflectivity features. The first number of each label represents the order in which the feature formed during the data analysis period. It is followed by either an R or an L denoting whether the feature moved down the right (southern) or left (northern) flank of the V-shaped radar echo, and the final number is the order in which the reflectivity feature moved down that particular flank. During the Dissipation Stage, features in the eastern portion of the radar echo were not identified because continuity of features was lost during a period of missing data from 2250 through 2305 CST. Border tick marks, indicating distances from CP-3 radar, are at 10 km intervals starting with the (x,y) values in bottom left corner. From Brown and Torgerson (2003).

characterized at mid- and upper-altitudes by a reflectivity maximum, or by a protrusion in maximum reflectivity contours. By keeping track of the reflectivity maximum in the vertical, and forward and backward in time, a four-dimensional history of the reflectivity feature was developed.

Evolution of reflectivity feature 9R4 was typical of updraft/downdraft cells found in the Carson storm (Fig. 2). At the earliest time of detection, feature 9R4 was barely detectable as it emerged from stronger reflectivities associated with mature updrafts in existence at that time. With time, reflectivity values increased at all heights until feature 9R4 reached its maximum vertical extent. During this period, strongest reflectivity values remained at mid-altitudes, suggesting that hydrometeors there were growing hailstones. Mid-altitude hydrometeors started to descend as the updraft and echo top were reaching their maximum vertical extents.

Reflectivity contours near the top of 9R4 ascended until about 2222 CST (Fig. 2). Contours ascending with time were evidence of an updraft in which hydrometeors were being produced and carried upward. Presence of an updraft also was indicated by Doppler velocity signatures of convergence near the ground and divergence in the upper portion of the cell. For most cells in the Carson storm, divergence near storm top was evident for approximately 4–6 minutes after the top of the reflectivity feature began its descent. With decreasing support for the updraft at lower heights, upward velocities eventually ceased, and the divergence pattern disappeared.

Descending contours (after time of maximum reflectivity at a given height) were evidence of hydrometeors descending toward the ground. As discussed in more detail in Section 4b, a Doppler velocity convergence signature was produced by air converging into the upper portion of the downdraft induced by descending hydrometeors. The signature was evident in the 8–10 km height interval during the first 15 minutes of hydrometeor descent (Fig. 2).

During the time that the updraft was growing, the reflectivity feature was oriented vertically (lower portion of Fig. 2). However, as the reflectivity feature (updraft portion of cell) was reaching its maximum vertical extent, it started to tilt to the right (i.e. south) with height-signaling already at this stage that hydrometeors associated with 9R4 would be moving down the storm's right flank. With time, tilt of the associated reflectivity feature eventually shifted to the downstream (or east-southeasterly) direction, and the feature moved more quickly toward the east-southeast in response to environmental winds that increased in speed with height. In contrast, a reflectivity feature that would move down the left flank of the storm would start to tilt to the left with height as it reached maximum vertical extent, and then tilt toward an easterly downstream direction after updraft demise.

Development of the Carson storm was divided into six stages (Brown and Torgerson 2003). These stages and their approximate times of existence are:

Initial Growth Stage	~2015–2039 CST
CG Lightning Stage	2039–2143 CST
Developing Hail Stage	2143–2217 CST
Large Hail Stage	2217–2250 CST
Dissipation Stage	2250–2325 CST
Orphan Anvil Stage	2325 CST & beyond

The first two stages occurred before the beginning of data collection with NCAR's CP-3 Doppler radar. Times for those stages were estimated from GOES-7 visible and infrared satellite data and from cloud-to-ground lightning strike data recorded by the National Lightning Detection Network. Times for the remaining four stages were based on CP-3 Doppler radar measurements.

Mid-altitude radar reflectivity patterns observed in the Carson storm varied during the last four stages of evolution (Fig. 3). During the Developing Hail Stage at 2211 CST, five reflectivity features (5L3, 6R3, 7L4, 8L5, and 9R4) at the upstream end of the storm were at various stages of updraft development. Features 5L3, 6R3, and 7L4 were in the main reflectivity core region, and the two newest ones formed a second group upstream of the first one. Brown et al. (2002) referred to these groupings of cells as "updraft clusters". The reflectivity pattern at 2235 CST shows the much more organized distribution of reflectivity features during Large Hail Stage. The overall reflectivity pattern was in the shape of a "V". During this stage of storm development, only one, or briefly two, updrafts (here 14L8 and 15L9) were in existence at a given time, with the newest updraft along the upstream edge of the echo. Features 5L3–9R4, which represented updrafts at the upstream end of the storm 24 min earlier, now represent columns of descending hydrometeors down-stream along the storm's flanks (feature 5L3 had descended below 5 km height by this time).

During the Dissipation Stage (Fig. 3), updrafts continued to form within the storm, but they were less energetic as each successive one grew to successively lower heights (see Fig. 6 in Part I; also Brown and Meitín 1994). The only labeled feature representing an updraft at 2310 CST was 21R9. The final stage of storm evolution was called the "Orphan Anvil Stage". Except for precipitation cores (associated with identifiable reflectivity features) settling out at lower altitudes, all that remained was a nondescript, three dimensional plume of radar echo. The plume extended 50-100 km downstream from the storm's previous updraft region. At low altitudes, the upstream end of the plume coincided with descending precipitation cores. With increasing altitude, the upstream end tilted downstream, as it responded to stronger winds aloft.

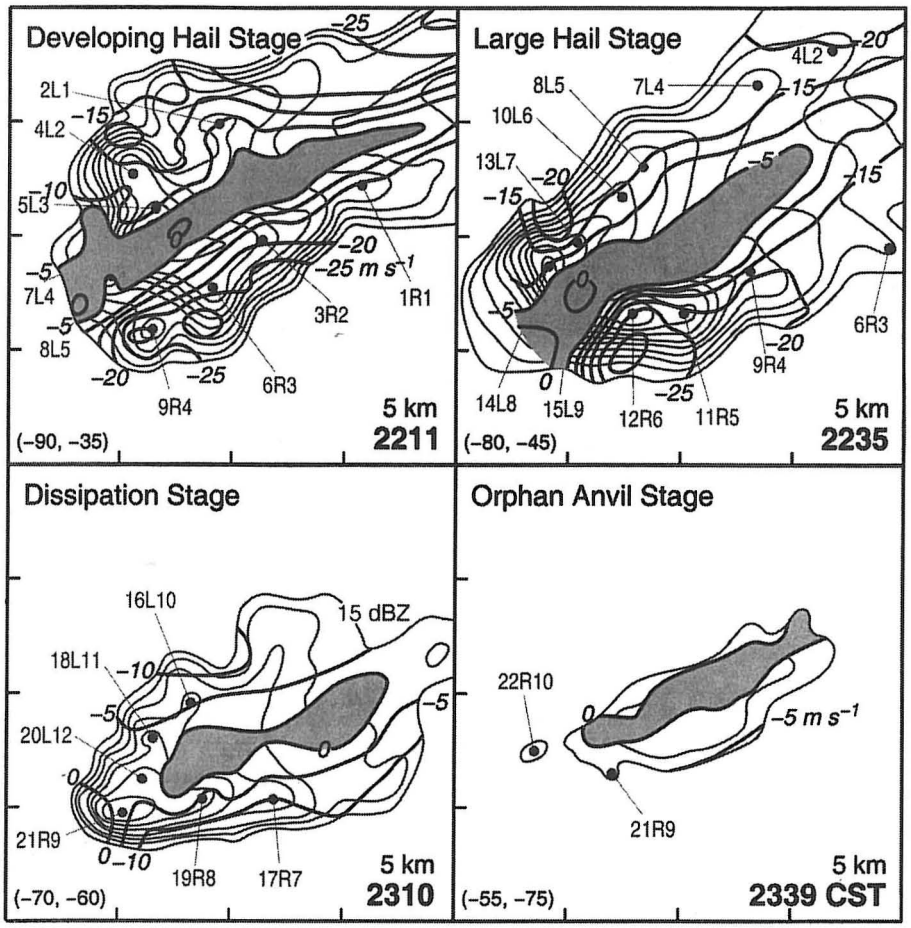

Fig. 4. Contoured CP-3 Doppler velocities at 5 km height superimposed on the reflectivity fields from Fig. 3. Negative (positive) Doppler velocities represent the component of within-storm flow toward (away from) the radar, which was located east to east-northeast of the storm. Contour interval is 5 m s^{-1}, with shading representing weak Doppler velocity values.

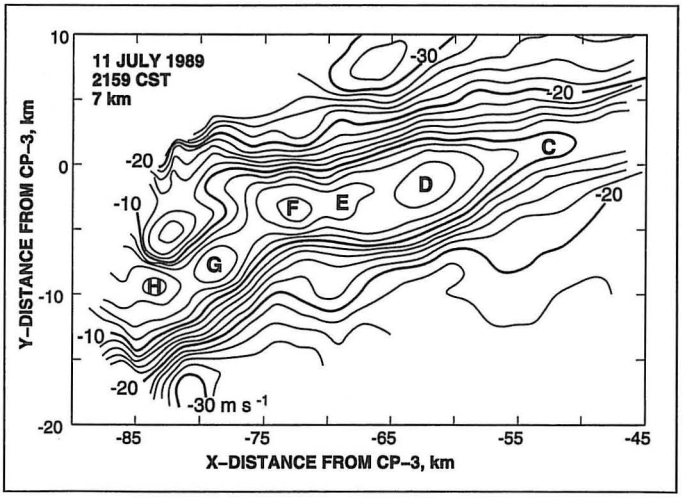

Fig. 5. Ground-relative Doppler velocity measurements in the Carson storm at 7 km height at 2159 CST. Contouring interval is 2 m s^{-1}, with thicker contours at 10 m s^{-1} intervals. Because flow has a major component toward the radar (located east-northeast of storm), all Doppler velocity measurements at this height and time are negative. Letters C–H represent identifiable wind speed minima that had spatial and temporal continuity; speed minima C–F formed prior to the beginning of Doppler radar data collection.

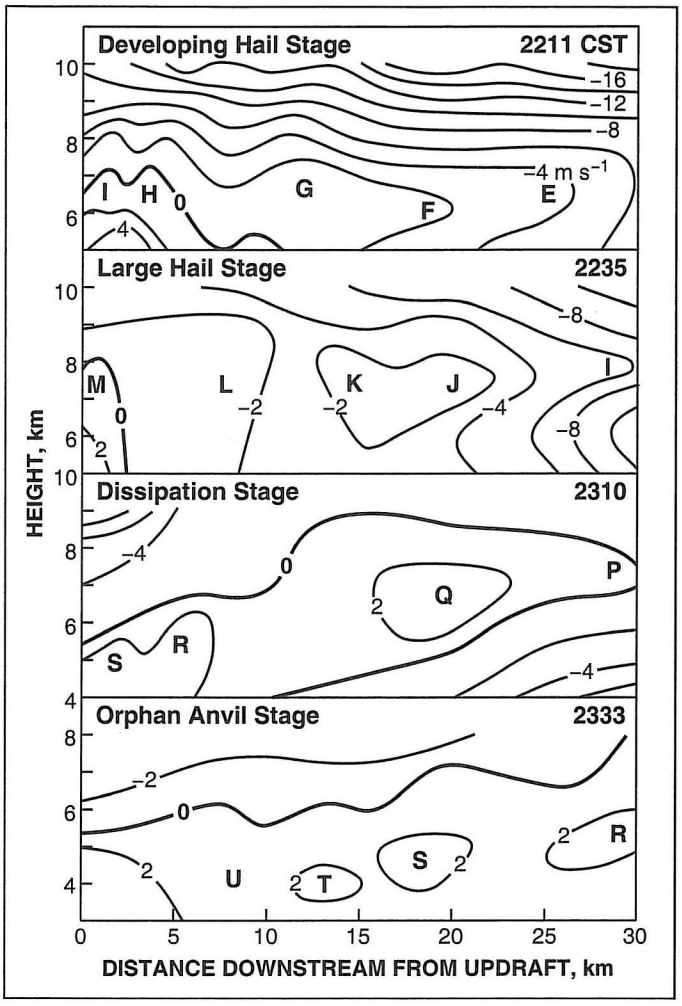

Fig. 6. Vertical cross-sections of Doppler velocity values through center of speed minima during four stages of storm development. Before being contoured in a vertical cross-section, data values were projected onto a mean speed minimum center line that was the best straight-line fit to the irregular center lines at various heights during a given volume scan. Horizontal distance was measured along the mean center line relative to the center of the reflectivity feature that represented the associated updraft; an estimated location for the no-longer existent updraft was used for the Orphan Anvil Stage. Centers of speed minima are indicated by letters; minima E and F formed before beginning of data collection and P and Q formed during the time period when the radar was not operating owing to a power failure.

The corresponding mid-altitude ground-relative Doppler velocity fields during the four stages are shown in Fig. 4. The overall characteristic was for weak Doppler velocities to extend along the central axis of the storm between the reflectivity maxima that produced the "V" shape of the storm. The strongest Doppler velocity values were found along the lateral flanks of the weak velocity region. During the Developing Hail and Large Hail Stages, the strongest velocities were concentrated on both sides of the high-reflectivity updraft region at the upstream end of the storm (representing the outer portions of a vorticity couplet).

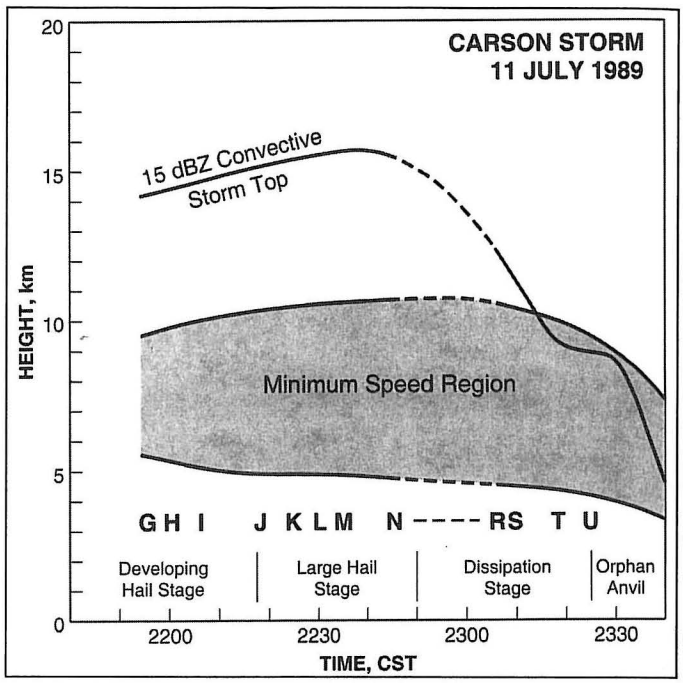

Fig. 7. Vertical and temporal extent of minimum speed region (shaded) in the Carson storm. For comparison purposes, the 15 dBZ top of the storm's convective region is indicated. Dashed portions of curves indicate missing data owing to a power failure. Letters represent the times that various wind speed minima first appeared. Vertical extent of the shaded minimum speed region was determined by the presence of an elongated region of weak Doppler velocities (in horizontal Doppler velocity cross-sections) bounded above by strong Doppler velocities and bounded below by the lack of an elongated region.

4. Characteristics of Mid-altitude Wake Flow Region

a. Doppler velocity minima[1]

The Doppler velocity fields in Fig. 4, contoured at 5 m s^{-1} intervals, show a rather uniform minimum speed region extending through the center of the storm. However, if one displays the Doppler velocity field using 2 m s^{-1} contour intervals, interesting details emerge. An example from early in the data collection period (Fig. 5, 2159 CST) reveals that localized speed minima (labeled C–H) were quite obvious at mid-altitudes along the center of the wake flow region. The minimum labeled H was associated with an updraft (reflectivity feature 4L2) in existence at that time (details about the relationship of speed minima with updrafts are discussed in Section 5). The downstream minima (G, F, E, D, and C) were associated with progressively older, former updrafts. Minimum ground-relative Doppler velocity values for D–H were all between -1 and -3 m s^{-1}.

On the lateral flanks of the speed minima, Doppler velocities reached values of -25 to -30 m s^{-1} or more, rep-

[1] The terms "Doppler velocity minimum", "Doppler velocity maximum", "speed minimum", and "speed maximum" refer to absolute values of Doppler velocity measurements.

resenting strong flow toward the radar. As a result, there were marked Doppler velocity gradients along the flanks with velocities increasing by 10–20 m s^{-1} over lateral distances of 2.5–5.0 km (producing average shear values of 3–5 x 10^{-3} s^{-1}). Ambient wind speed at 7 km height was about 17 m s^{-1} and its direction was within 10–15° of the radar viewing direction, so the Doppler component of the ambient wind was -16.5 to -17 m s^{-1}. Consequently, Doppler velocities along the center of the wake region were about 15 m s^{-1} weaker than the ambient flow and those along the outer edges were up to about 15 m s^{-1} stronger.

To indicate the vertical extent of the minimum speed region, vertical cross-sections were constructed through the speed minima along the center of the wake region during four stages of storm evolution (Fig. 6). The minimum speed region typically was vertically aligned and oriented toward 060–070°. However, there was a time period from 2223 through 2246 CST, roughly corresponding to the Large Hail Stage, when its orientation rotated slightly clockwise with height. During the Dissipation and Orphan Anvil Stages, the wake region tilted slightly downward in the upstream direction. The tilt arose owing to new updrafts during the Dissipation Stage growing to successively lower heights, and therefore, the associated speed minima formed at lower heights. No new updrafts formed during the Orphan Anvil Stage and so the wake region was no longer being regenerated at the upstream end. Temporal variation of the overall depth of the minimum speed region is shown in Fig. 7.

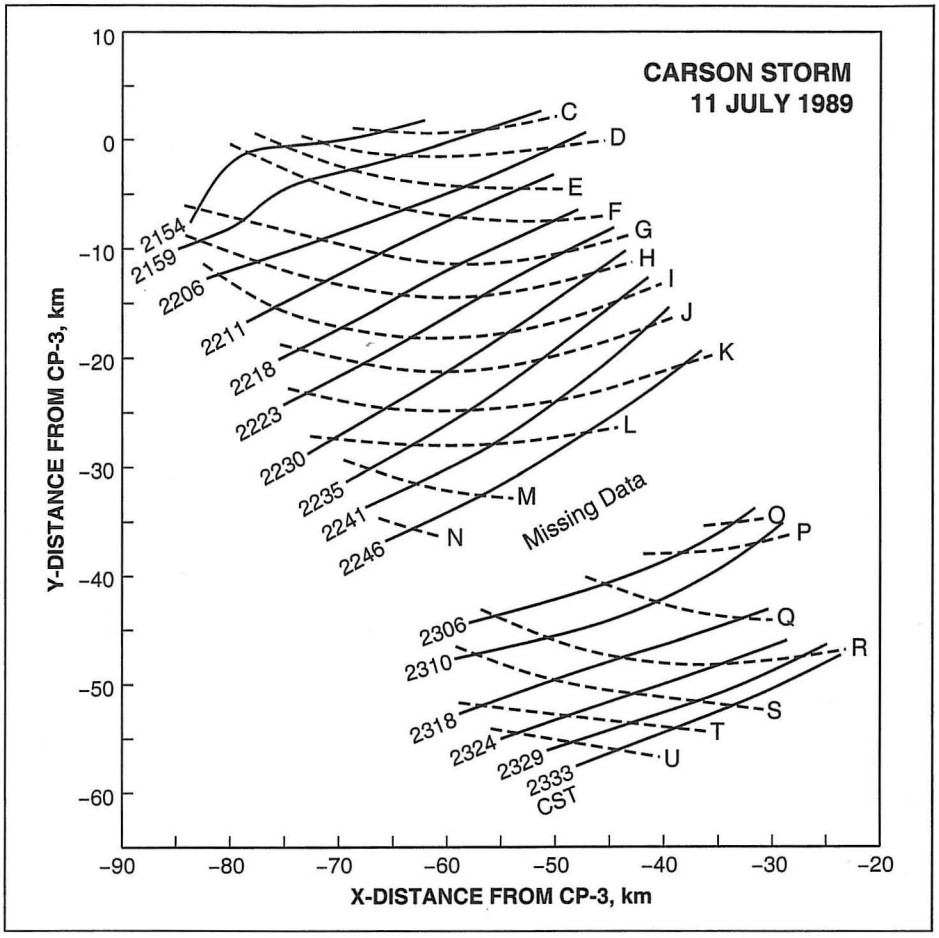

Fig. 8. Movement of wind speed minima C–U (dashed curves) downstream through the center of the wake flow region at a height of 7 km before the missing data break and 6 km then 5 km after the break. Each solid curve, where it intersects the dashed curves, indicates locations of respective minima at a given time. Minima C–F formed prior to radar data collection. Minima O–Q formed during the missing data period; minimum O or P could have been a continuation of N.

Mid-altitude minima exhibited continuity as they moved downstream through the wake region (Fig. 8). A given isochrone represents a smoothed centerline of minimum wind speeds in the wake region. The dashed curves indicate that minima were identifiable for 25–30 minutes or more. In a dual-Doppler radar study of a small severe storm, Brown (1989) found that mid-altitude minima in the wake region of that storm were identifiable for comparable periods of time. As illustrated schematically in Fig. 9, the east-northeast orientation of the wake region was a consequence of localized minima moving essentially to the east, while the storm and region of new updraft initiation was moving to the southeast.

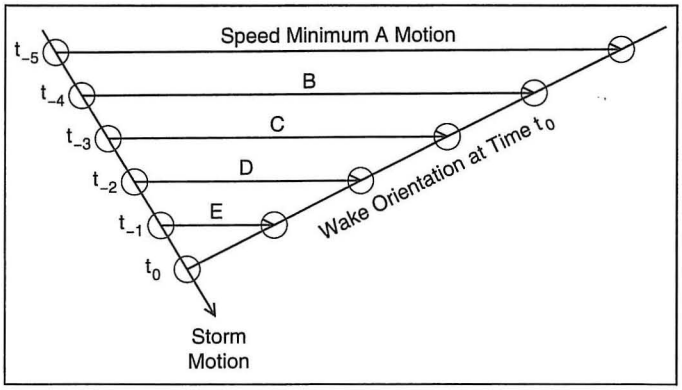

Fig. 9. Idealized schematic interpretation of the curves in Fig. 8. Orientation of wake region at time t0 arises from earlier speed minima moving with the ambient flow.

b. Doppler velocity maxima

The mid-altitude Doppler velocity fields in Figs. 4 and 5 document strong velocity gradients along the lateral flanks of the minimum speed region, with pronounced speed maxima on the flanks of the updraft region at the west-southwest end of the storm. Some maxima disappeared after they started moving downstream. However, most of them maintained their identities for tens of minutes.

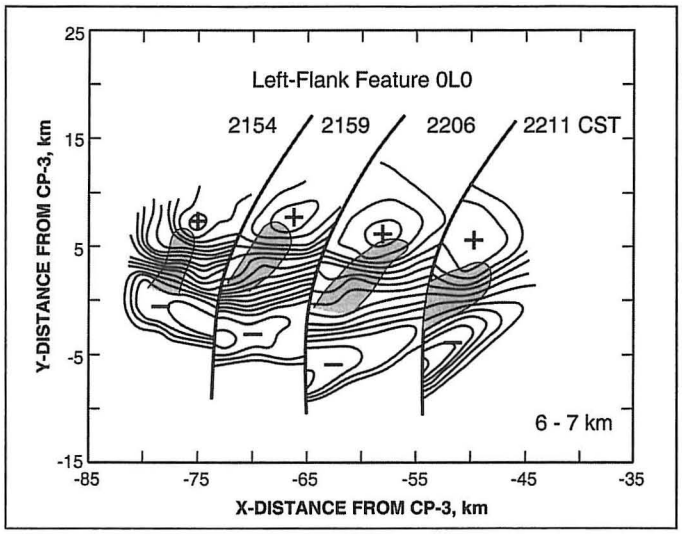

Fig. 10. Evolution of Doppler velocity field associated with left flank reflectivity feature 0L0 (shaded region) in the 6–7 km height interval. Left-flank speed maximum is indicated by a plus sign (+) and low-speed central portion of wake region is indicated by a minus sign (-). Contour interval is 2 m s^{-1}.

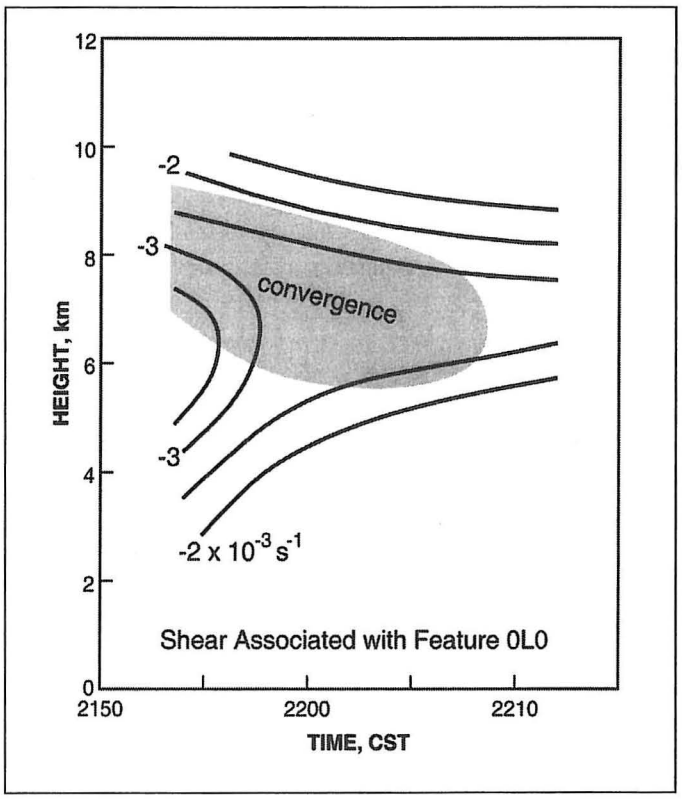

Fig. 11. Time-height plot of left-flank horizontal shear region associated with feature 0L0. Contours represent smoothed values of shear computed between the extreme Doppler velocity values like those shown in Fig. 10. Shading indicates the presence of a small region of convergence within the shear region.

At the top center of Fig. 5 is a -33 m s^{-1} Doppler velocity maximum (that is, maximum flow toward the radar). Tracing the maximum backward, it was found to be in existence when CP-3 data collection started at

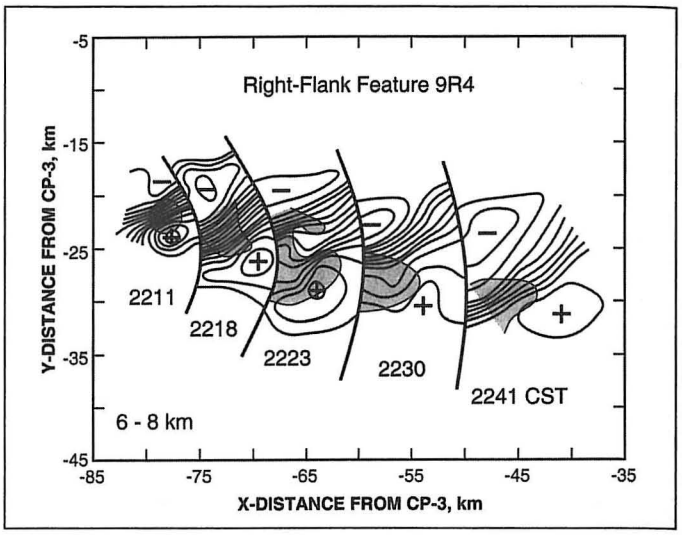

Fig. 12. Same as Fig. 10, except for evolution of right-flank feature 9R4 in the 6–8 km height interval. Owing to overlapping fields, data for 2235 CST are not displayed.

the reference time of 2154 CST. Movement of the maximum (plus sign) is shown in Fig. 10, along with Doppler velocity contours in the northern portion of the wake region. Superimposed on the velocity field is a shaded left-flank reflectivity feature that moved along with the speed maximum. Following our naming convention, the left-flank feature is called 0L0 because it was associated with an updraft that occurred prior to beginning of data collection.

To investigate evolution of horizontal shear associated with a speed maximum, a crude estimate of shear (S) was computed from

$$S = \Delta V / D .$$

In the equation, D is the minimum distance between the center of the speed maximum and the axis of speed minima extending through the center of the wake region, and ΔV is the Doppler velocity difference across that distance. For anticyclonic speed shear, ΔV was defined as negative. Horizontal shear associated with feature 0L0 was identifiable primarily at mid-altitudes (Fig. 11). Shear was strongest at the beginning of data collection when the speed maximum was already downstream of the updraft region. Following a fairly rapid decrease in strength, the magnitude and vertical extent of shear decreased more slowly with time as the feature moved downstream out of the data analysis region.

In Fig. 10, the reflectivity feature represents the later stage of cell evolution where hydrometeors that had been in the middle and upper portions of the cell's updraft are descending following updraft demise. One would expect mid- to upper-altitude air to be converging into the upper portions of the downdraft induced by the descending hydrometeors. Indeed, the S-shaped Doppler velocity contours and decreased gradient within the reflectivity feature at 2159 and 2206 CST represent the pattern that would

Table 1. Summary of reflectivity feature (updraft/downdraft cell) characteristics. Individual reflectivity features that caused ambient flow to be diverted around them and thereby affected the tilt and movement of nearby features (updraft/downdraft cells) were identified from data used to produce Fig. 13 in Part I. Dashed line indicates missing data gap, after which new updrafts grew to lesser and lesser heights.

Reflectivity Feature	Location in Updraft Region		Induced Divergent Flow	Associated with Downstream Minimum	Associated with Downstream Maximum
	Center	Flank			
2L1	X			G	
3R2		X	X		X
4L2	X		X	H, I	
5L3		X	X		
6R3		X			X
7L4	X		X		
8L5	X		X		
9R4		X	X		X
10L6	X		X	J, K	
11R5		X	X		X
12R6	X		X	L	
13L7		X			X
14L8		X			X
15L9	X		X	M	
16L10		X			X
17R7		X			X
18L11	X			R	
19R8		X			X
20L12	X			S	
21R9	X			T	
22R10	X			U	

be produced by axisymmetric convergence within an anticyclonic shear region. Superimposed on the shear contours in Fig. 11 is the shaded height and time interval over which the convergence signature occurred. The height of convergence slowly decreased with time along with the descending column of hydrometeors.

An example of a right-flank speed maximum, the one associated with reflectivity feature 9R4 (see Fig. 2), is shown in Fig. 12. Relationship of the reflectivity feature to the extreme Doppler velocity values is similar to that in Fig. 10, with the reflectivity feature being closer to the maximum than the minimum at later times. Feature 9R4 developed in the mid-altitude cyclonic shear region along the right (south) side of the updraft region, and remained within the shear region during its lifetime. Based on the compact shear region at the location of feature 9R4 at 2211 CST, it is possible that low- to mid-altitude convergence into the updraft associated with 9R4 initially concentrated shear along the right side of the wake region to produce a rotating updraft at midaltitudes (e.g., Brown 1992). A rotating updraft is deduced when vertical velocity and vertical vorticity are positively correlated (e.g., Davies-Jones, 1984).

As the updraft associated with feature 9R4 died, air converging into the upper portions of the downdraft (induced by descending hydrometeors) would have taken over as the concentrating agent of the local shear. Convergence produced the backward S-shaped Doppler velocity contours at 2223 and 2230 CST at the altitudes displayed in Fig. 12. The backward S-shaped contours are consistent with those produced by axisymmetric convergence within a cyclonic shear region. The shaded reflectivity feature at 2223 CST exhibited a localized reflectivity minimum (indented boundary) near the convergence signature. It is possible that the indented minimum was produced when lower-reflectivity particles (smaller hydrometeors and/or lesser concentration of hydrometeors) from higher altitudes descended with the downdraft, and displaced the higher reflectivity particles found in that region. At other times and heights, there was either a minimum or a broad area of constant reflectivity associated with the convergence signature.

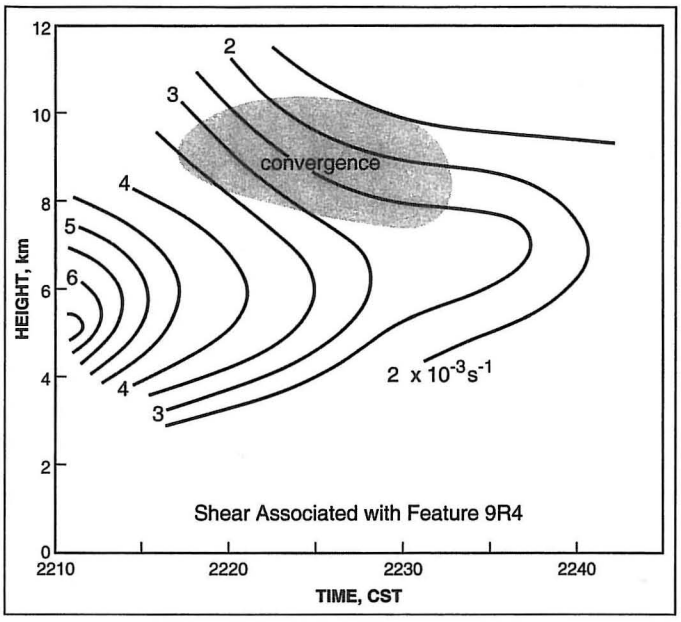

Fig. 13. Same as Fig. 11, except for the right-flank horizontal shear region associated with feature 9R4.

The time-height distribution of horizontal shear associated with feature 9R4 (Fig. 13) shows that the most intense shear occurred as the updraft associated with 9R4 was in its initial growth stage (left portion of Figs. 2 and 13). Convergence into the lower portion of the updraft likely concentrated ambient shear, producing the shear maximum found in the 4–7 km height interval. Prior to 2220 CST, as 9R4 was reaching its maximum vertical extent, the reflectivity feature was dominated by a growing updraft. However, before 9R4 reached its maximum height, hydrometeors at middle and upper altitudes started to descend (Fig. 2). Air converging into the upper portions of the induced downdraft produced the convergence region documented in Figs. 2 and 13. Convergence signatures lasted for about 15 minutes, lowering slightly with time.

5. Overview of Flow Features

In order to investigate the relationship of flow field features with the updraft region, a composite presentation (Fig. 14) was prepared at the time that each new speed minimum became prominent. The composite combines updraft information (deduced from reflectivity and Doppler velocity signatures) with the mid-altitude Doppler velocity field. Listed in Table 1 are some of the characteristics of the reflectivity features that were associated with speed minima and speed maxima.

The consistent pattern shown in Fig. 14 is that speed maxima (blue) occurred on lateral edges of the shaded updraft region (red) and that speed minima were in the immediate vicinity of individual updrafts (gray). Movement of individual speed minima downstream relative to the updraft region are evident in the figure.

Cyclonic shear dominated the right (southern) part of the updraft region and anticyclonic shear dominated the left (northern) part. Shear was most pronounced during the Large Hail Stage (2217–2250 CST) when the tallest, and presumably strongest, updrafts in the storm occurred (see Fig. 6 in Part I). Even though individual speed maxima moved downstream from the updraft region, the shear regions remained.

About half of the updrafts formed in the strong shear regions on the lateral flanks of the updraft region, while the other half formed in the minimum shear region in between (Table 1). Those updrafts on the flanks were associated with concentration of the lateral shear (vertical vorticity) and with speed maxima at the edges of the updraft region. Of the 10 updrafts that formed in the shear regions (six on the right, four on the left), nine were associated with Doppler velocity maxima that moved down the right or left storm flank. Feature 5L3 did not have an apparent maximum associated with it (Table 1). Examples of speed maxima that moved downstream with updraft/downdraft cells were shown in Figs. 10 and 12.

Those updrafts that formed in the minimum shear region were associated with speed minima (Table 1). The initial appearance of a wind speed minimum in Fig. 14 is based on the reference time of a radar volume scan, and not on the time that the minimum formed. Therefore, the minimum could have been in existence for several minutes before the reference time. In order to help interpret the relationship of stage of updraft development to the initial appearance of a speed minimum, the time of initial appearance of each minimum was plotted relative to the peak of a 15-dBZ echo top curve for a typical reflectivity feature (Fig. 15).

Minima "G" and "H" were the only minima that were exactly coincident with the updraft signatures (Fig. 14); i.e., there were no downstream extensions of the Doppler velocity contour lines—as contrasted with minima such as "J" or "K" – whose contours did extend downstream. Minima "G" and "H" initially appeared at reference times when the associated updrafts were strongest (Fig. 15). When a speed minimum coincides with an updraft, the minimum likely represents low-momentum, low-altitude air that was transported upward by the updraft (e.g., Davies-Jones 1974; Gray et al. 1975; Fankhauser et al. 1992). Winds in the lowest 2 km were less than 2–3 m s^{-1} (Fig. 1), so it is possible that the coincident minimum reflects the presence of low-altitude air at mid-altitudes in the updraft.

The other minima initially appeared at reference times that occurred during the weakening stages of updrafts, where the rate of rise of the reflectivity contour decreased with time or started to descend (Fig. 15). The Doppler velocity contours associated with these minima encompass at least part of the updraft signature, but they also extend some distance downstream (Fig. 14). The downstream extension of a minimum likely represents the presence of a low-pres-

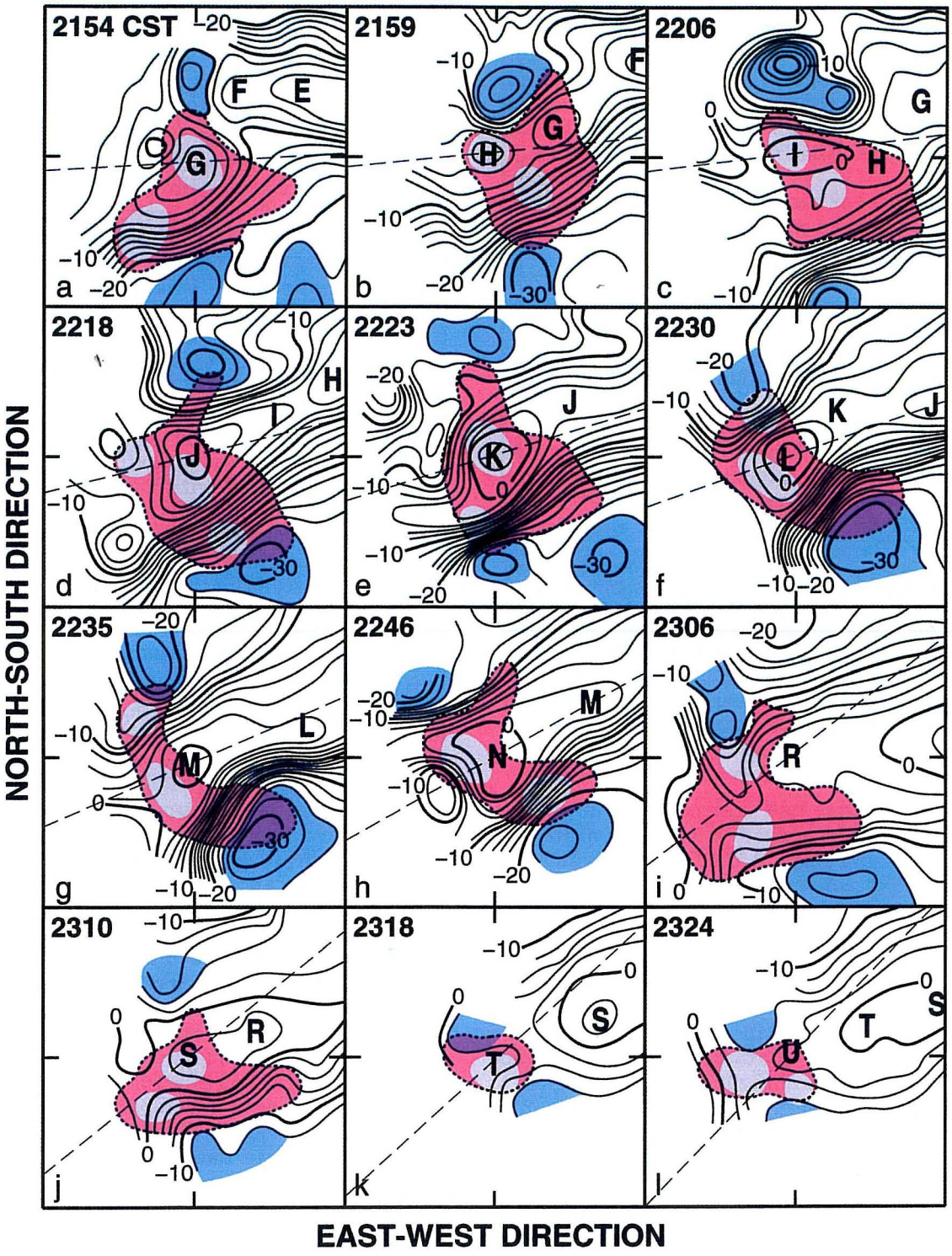

Fig. 14. Evolution of Doppler velocity fields at mid-altitudes in the Carson storm. Panels show ground-relative Doppler velocity fields at the reference times that speed minima G–N and R–U first became apparent; the gap arose owing to loss of data during a power outage. R evidently formed during the missing data period prior to 2306 CST. Reflectivity features (updrafts) associated with the minima are indicated in Table 1; minimum N was associated with one of the rapidly evolving updrafts whose evolution could not be resolved owing to missing data following 2246 CST. Through 2246 CST, display heights are 6–8 km; thereafter heights are 5–7 km. Each panel is a 20 km x 20 km square centered on the location where each new midaltitude speed minimum (capital letter) first appeared. Red shaded areas represent the nominal updraft region (50 dBZ and greater through 2246 CST then decreasing to 25 dBZ by 2324 CST), with gray shading indicating reflectivity features associated with growing updrafts. Blue shaded areas indicate localized wind speed maxima on flanks of updraft region. Dashed line in each panel is radial line (viewing direction) from the radar westward/southwestward through center of localized speed minimum. Since the radar viewing direction was within ±20° of the orientation of wake centerline, single-Doppler velocity measurements accurately portray the Doppler component of the dominant flow in the overall wake region.

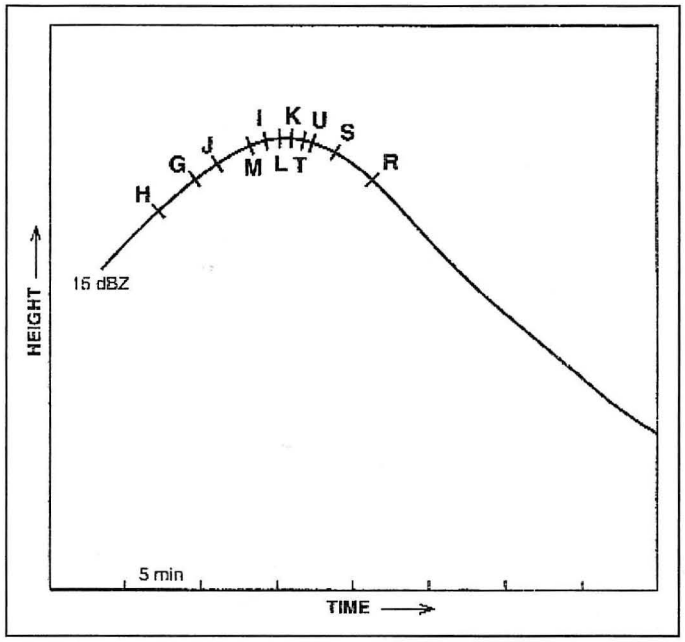

Fig. 15. Position during lifetime of a typical reflectivity feature (represented by echo top height of 15 dBZ, like that shown in Fig. 2) when identified midaltitude wind speed minima (capital letters) first appeared. Minimum N is not plotted because it was associated with an unnamed short-lived reflectivity feature, and therefore, the portion of the feature lifetime when N appeared could not be determined. Minimum R formed sometime during the 20 minute period of missing data prior to 2306 CST.

sure wake region that had started to form on the downstream side of the updraft when the updraft was in its strong growing stage. After flowing around the updraft, air likely converged into the low-pressure region and descended to the ground (e.g., Knupp and Cotton 1982; Brown 1989). As the updraft died, the part of the speed minimum associated with vertical transport of low-altitude air disappeared. The remaining portion of the minimum moved downstream where it retained its identity for up to 30 minutes (e.g., Fig. 8) as air continued to flow into and descend within the weakening low-pressure region.

As indicated in Table 1, two updrafts (4L2 and 10L6) had two speed minima associated with them. Evidently, in each case the low-pressure region on the downstream side of the updraft broke away and moved downstream while the updraft was still in existence. Then a second low-pressure region formed and it moved downstream later following updraft demise.

The fact that mid-altitude air flows around strong thunderstorm updrafts is evident from flow fields derived from dual-Doppler measurements (e.g., Knupp and Cotton 1982; Brown 1989; Brown and Meitín 1994). The dual-Doppler study by Brown (1989), for example, reveals that trajectories of storm-relative air converged into the wake low and reversed direction back toward the updraft—producing the wind speed minimum—as they descended toward the ground. As the mid-altitude speed minimum moved downstream following updraft demise, the minimum maintained its identity with mid-altitude air continuing to converge into it. With time, a train of slowly weakening wind speed minima extended from the updraft region toward and through the downstream end of the storm.

Based on the foregoing discussions, we presume that a Doppler velocity minimum in the Carson storm initially coincided with a growing updraft (transporting air with low horizontal momentum upward). For those updrafts that formed in the central weak shear region, a mid-altitude wake low would have developed on the downstream side of the updraft by the time the updraft was reaching its maximum vertical extent and starting to weaken. Consequently, the speed minimum became elongated, representing the transition from a disappearing minimum associated with the cessation of vertical transport of low-altitude air within the dying updraft to a strengthening minimum associated with the developing wake low. Following updraft demise, the minimum would represent a slowly weakening wake low that moved downstream with mid-altitude air continuing to converge into it and descend to the ground.

6. Discussion

By combining reflectivity and single-Doppler velocity measurements in the Carson hailstorm, we deduced interesting details about interactions between updrafts and the ambient wind field. During the growth stage, individual updrafts (with their strong vertical momentum) remained erect even in the presence of vertical shear of the horizontal wind. With an updraft cell moving with the mean wind, upper-altitude air would then be forced to flow around the updraft. This characteristic was documented in Fig. 13 of Part I where it was shown that the appearance of a new updraft caused the previous updraft to start moving to the left or right, depending on whether the previous updraft was on the left or right flank of the new updraft.

All updrafts formed at the upwind end of the storm and there typically were two or more updrafts (at various stages of development) in existence within the updraft region at a given time. The updraft region as a whole had a marked influence on the overall flow pattern as revealed by the Doppler velocity measurements. Maximum speeds (exceeding the ambient winds by 10–15 m s^{-1}) occurred on the left and right flanks of the updraft region, with a band of very weak speeds found in between. The overall pattern resembled the Doppler velocity signature of a vorticity couplet, with cyclonic shear in the right portion of the updraft region and anticyclonic shear in the left portion. Instead of being associated with an individual updraft (e.g., Rotunno 1981), the vorticity couplet was associated with the entire updraft region.

About half of the updrafts formed in the weak speed region and the other half formed within the areas of strong shear in the outer portions of the

updraft region (Table 1). Those that formed in the weak speed region exhibited characteristics that were not apparent in those that formed in the shear regions. Doppler velocity minima in the weak speed region coincided with the centers of the updraft signatures during the updraft growth stage. A speed minimum within the updraft is interpreted to represent low-altitude, low-momentum air transported upward by the updraft. With time, the minimum became elongated in the downstream direction, and then broke away from the dying updraft, moving downstream. It is hypothesized that the elongation was due to air flowing around the strong updraft and converging into a developing wake low-pressure region where it reversed flow direction back toward the updraft as it descended toward the ground. After the updraft died, the low-pressure region (with air continuing to converge into it) was free to move downstream.

When an updraft formed in one of the shear regions, the associated speed minimum was not evident owing to the strong velocity gradient across the updraft; flow nevertheless was being diverted by the updraft as indicated by the divergent motion of adjacent older updrafts in Fig. 13 of Part I, and as indicated in Table 1. As the updraft grew through the shear region, it is hypothesized that convergence into the updraft concentrated the ambient vorticity, and produced a packing of the Doppler velocity isotachs (Fig. 14) that suggested mid-altitude updraft rotation (e.g., Brown 1992). The associated Doppler velocity maximum subsequently moved downstream with the updraft/downdraft cell.

It would be enlightening to use the results of this study to evaluate the theoretical and empirical hypotheses that were discussed in the introduction. The theoretical hypotheses depend on the favored orientation of horizontal vortex tubes (defined as being perpendicular to the vertical shear of the low-altitude horizontal wind and as being positive to the left of the shear vector). Based on the hodograph in Fig. 1 (where updraft motion is approximated by the mean wind vector), updraft-relative winds in the lowest 2.5 km of the environment exhibited negative crosswise vorticity, while winds in the 2.5-4.0 km layer exhibited a major component of negative steamwise vorticity (see, e.g., Doswell 1991 for interpretation of hodographs).

The Rotunno (1981) version of the theoretical hypothesis states that as a horizontal vortex tube aligned perpendicular to the low-altitude, storm-relative inflow (positive crosswise horizontal vorticity) approaches a thunderstorm updraft, it is lifted by the updraft, forming an inverted "U" shape surrounding the top and sides of the updraft. The portion of the tube on the right side (looking downstream) represents cyclonic vertical vorticity, and the portion of the left side represents anticyclonic vertical vorticity—producing a vorticity couplet on the lateral flanks of the updraft. Of the different vortex tube orientations present in the lowest 4 km of the Carson storm environment, none of them represent the presence of positive crosswise vorticity. In the storm, a vorticity couplet occurred on the flanks of the entire updraft region (consisting of updrafts at various stages of development). Although there was evidence that individual updrafts perturbed the ambient flow, none of the updrafts had obvious vorticity couplets associated with them.

A question arises whether it is more logical for the horizontal vortex tube to be *lifted by the updraft* or to be *drawn up into the updraft*. In the latter situation, the cyclonic and anticyclonic portions of the vertical tube would be adjacent to each other, and cancel each other to produce zero net vertical vorticity in the updraft. Consequently a vorticity couplet would not be evident on the lateral flanks of the updraft.

Davies-Jones' (1984) theoretical model visualizes a hump occurring in otherwise horizontal isentropic surfaces. A vorticity couplet is produced on the lateral flanks of the hump when storm-relative air having low-altitude, positive crosswise horizontal vorticity passes up over the top of the hump. An updraft is produced when air flows up the surface of the hump, and a downdraft is produced when air flows down the downstream side. According to the Davies-Jones model, the vorticity couplet then should be on the flanks of the hump midway between the updraft and downdraft. However, as shown in Fig. 14, the vorticity couplet in the Carson storm is consistently on the flanks of the updraft region only.

The Davies-Jones model also predicts that when updraft-relative air having low-altitude positive streamwise horizontal vorticity (vortex lines parallel to updraft-relative inflow air) is drawn up into an updraft, the vortex lines are tilted upward producing cyclonic updraft rotation (positive correlation between vertical velocity and vertical vorticity fields). Anticyclonic updraft rotation would occur if negative streamwise horizontal vorticity were drawn up into an updraft. One can argue that several of the individual updrafts in Fig. 14 have mid-level rotation because the vertical velocity (gray reflectivity features), and vertical vorticity (local packing of Doppler velocity contours) fields are correlated. In particular, anticyclonic rotation is most evident in the left-flank updraft at 2230 CST, and cyclonic rotation is most evident in the right-flank updrafts at 2223 and 2246 CST, as well as in the right-flank updraft associated with feature 9R4 at 2211 CST in Fig. 12. Therefore, in order to explain what was observed in the Carson storm, low-altitude flow approaching one portion of the updraft region must contain positive crosswise horizontal vorticity; flow approaching another portion must contain positive streamwise horizontal vorticity; and flow approaching yet another portion must contain negative streamwise horizontal vorticity—an unrealistic combination of low-altitude flow conditions. Since the model does not consistently explain the observations, it would appear that a linear theory representing shallow convection in a dry atmos-

phere does not adequately represent non-linear processes associated with actual deep convection in a moist environment.

Based on many of the empirical studies (especially the earlier ones) discussed in the introduction, the prevailing concept is that the mid-altitude vorticity couplet arises when a mature updraft partially blocks the mid-altitude environmental flow. This Doppler radar study of the Carson storm and some of the other Doppler radar studies indicate a slightly different picture. It is the entire updraft region that has the vorticity couplet associated with it. Evidently, the vertical momentum of individual updrafts collectively presented enough resistance to the approaching environmental flow that air slowed down as it flowed through the porous updraft region. As air farther upstream approached the wall of slower-moving air (producing a region of higher pressure), some of the air was diverted, increasing speed as it flowed around the sides of the updraft region. Even though individual updrafts in the Carson storm were growing and dying, the updraft region as a whole diverted some of the mid-altitude flow and continued to produce the overall vorticity couplet for several hours as the storm propagated southeastward.

In conclusion, the mid-altitude vorticity couplet on the right and left flanks of the Carson storm appeared to be a result of the interactions of mid-altitude ambient flow with the overall updraft region. The vorticity couplet did not appear to be due to vertical tilting of low-altitude horizontal vortex tubes by an updraft, or by a hump in isentropic surfaces as proposed in the theories presented by Rotunno (1981) and Davies-Jones (1984), respectively. Neither theory was supported by the environmental hodograph and the Doppler radar signatures associated with the Carson storm.

Acknowledgments

This research was supported in part through Cooperative Agreement NA47RA0184 from the NOAA Federal State Cooperative Program in Atmospheric Modification Research to the North Dakota Atmospheric Resource Board (NDARB). We are grateful for the continuing interest of Bruce Boe, past Director of NDARB and Director of the North Dakota Thunderstorm Project. John Helsdon (South Dakota School of Mines & Technology) provided the inspiration for studying this storm by recognizing the storm's existence and calling in Bob Bowie and his crew (NCAR), who conscientiously collected the CP-3 radar data. John Hirsch (SDSM&T) provided sounding data. Bob Rilling (NCAR) kindly provided us with CP-3, PAM, and CLASS data sets. Joan O'Bannon (NSSL) skillfully prepared the figures. We appreciate the comments of Kim Elmore and Vincent Wood (NSSL) on preliminary drafts of this manuscript. Reviewers Bradford Herold (NWS, Barrow, AK) and Richard Dixon (Texas State University) provided helpful suggestions for improving the manuscript.

Authors

Rodger Brown has been a research meteorologist at the NOAA/National Severe Storms Laboratory since 1970. He has been involved with various aspects of Doppler radar ranging from a) severe storm studies, to b) understanding of Doppler velocity signatures in severe storms through simulations (in collaboration with Vincent Wood), and to c) development of refined WSR-88D scanning strategies that provide greater spatial and temporal resolution of convective storms (in conjunction with the WSR-88D Radar Operations Center). Previously, he worked at the Mount Washington Observatory, Blue Hill Meteorological Observatory, for the U.S. Weather Bureau at the Severe Local Storms Research Unit and at Little America V, Antarctica, Cornell Aeronautical Laboratory, and Wave Propagation Laboratory. He earned a B.S. degree in Earth Sciences from Antioch College, M.S. in Geophysical Sciences from the University of Chicago, and Ph.D. in Meteorology from the University of Oklahoma.

Kathleen Torgerson has been a forecaster with the NOAA/National Weather Service Weather Forecast Office (WFO) at Pueblo, Colorado since 1998, where her program responsibilities include radar and the Interactive Forecast Preparation System. Previously, she worked as a meteorologist intern at WFO Pueblo, and WFO Denver. She graduated from the University of Oklahoma in 1994, where she earned a B.S. degree in Meteorology. While an undergraduate student, she worked at the NOAA/National Severe Storms Laboratory as a meteorological technician.

References

Bluestein, H. B., and G. R. Woodall, 1990: Doppler-radar analysis of a low-precipitation severe storm. *Mon. Wea. Rev.*, 118, 1640–1664.

Boe, B. A., and Coauthors, 1992: The North Dakota Thunderstorm Project: A cooperative study of High Plains thunderstorms. *Bull. Amer. Meteor. Soc.*, 73, 145–160.

Brown, R. A., 1989: Initiation and propagation of thunderstorm mesocyclones. Ph.D. dissertation, University of Oklahoma, 321 pp. [Available from University Microfilms, Ann Arbor, MI, No. 89-19983.]

_____, 1992: Initiation and evolution of updraft rotation within an incipient supercell thunderstorm. *J. Atmos. Sci.*, 49, 1997–2014.

_____, and K. C. Crawford, 1972: Doppler radar evidence of severe storm high-reflectivity cores acting as obstacles to airflow. Preprints, *15th Radar Meteor. Conf.*, Champaign-Urbana, IL, Amer. Meteor. Soc., 16–21.

_____, and V. T. Wood, 1991: On the interpretation of single-Doppler velocity patterns within severe thunderstorms. *Wea. Forecasting*, 6, 32–48.

_____, and R. J. Meitín, 1994: Evolution and morphology of two splitting thunderstorms with dominant left-moving members. *Mon. Wea. Rev.*, 122, 2052–2067.

_____, and K. L. Torgerson, 2003: Interpretation of single-Doppler radar signatures in a V-shaped hailstorm: Part I - Evolution of reflectivity-based features. *Natl. Wea. Dig.*, 27, 3–14.

_____, C. R. Safford, S. P. Nelson, D. W. Burgess, W. C. Bumgarner, M. L. Weible, and L. C. Fortner, 1981: Multiple Doppler radar analysis of severe thunderstorms: Designing a general analysis system. NOAA Tech. Memo. ERL NSSL 92, Nat. Severe Storms Lab., Norman, 21 pp. [NTIS PB82-114117.]

_____, C. A. Kaufman, and D. R. MacGorman, 2002: Cloud-to-ground lightning associated with the evolution of a multicell storm. J. Geophys. Res., 107 (D19), 4397, doi:10.1029/2001JD000968.

Browning, K. A., and G. B. Foote, 1976: Airflow and hail growth in supercell storms and some implications for hail suppression. *Quart. J. Roy. Meteor. Soc.*, 102, 499–533.

Cressman, G. P., 1959: An operational objective analysis scheme. *Mon. Wea. Rev.*, 87, 367–374.

Davies-Jones, R. P., 1974: Discussion of measurements inside high-speed thunderstorm updrafts. *J. Appl. Meteor.*, 13, 710–717.

_____, 1984: Streamwise vorticity: The origin of updraft rotation in supercell storms. *J. Atmos. Sci.*, 41, 2991–3006.

_____, C. A. Doswell III, and H. E. Brooks, 1994: Comments on "Initiation and evolution of updraft rotation within an incipient supercell thunderstorm." *J. Atmos. Sci.*, 51, 326–331.

Dennis, A. S., C. A. Schock, and A. Koscielski, 1970: Characteristics of hailstorms of western South Dakota. *J. Appl. Meteor.*, 9, 127–135.

Doswell, C. A., III, 1991: A review for forecasters on the application of hodographs to forecasting severe thunderstorms. *Natl. Wea. Dig.*, 16 (1), 2–16.

Eagleman, J. R., and W. C. Lin, 1977: Severe thunderstorm internal structure from dual-Doppler radar measurements. *J. Appl. Meteor.*, 16, 1036–1048.

Fankhauser, J. C., 1971: Thunderstorm-environment interactions determined from aircraft and radar observations. *Mon. Wea. Rev.*, 99, 171–192.

_____, G. M. Barnes, and M. A. LeMone, 1992: Structure of a mid-latitude squall line formed in strong unidirectional shear. *Mon. Wea. Rev.*, 120, 237–260.

Foote, G. B., and H. W. Frank, 1983: Case study of a hailstorm in Colorado. Part III: Airflow from triple-Doppler measurements. *J. Atmos. Sci.*, 40, 686–707.

Fujita, T., and H. Grandoso, 1968: Split of a thunderstorm into anticyclonic and cyclonic storms and their motion as determined from numerical model experiments. *J. Atmos. Sci.*, 25, 416–439.

Gray, G. R., R. J. Serafin, D. Atlas, R. E. Rinehart, and J. J. Boyajian, 1975: Real-time color Doppler radar display. *Bull. Amer. Meteor. Soc*, 56, 580–588.

Heymsfield, G. M., 1978: Kinematic and dynamic aspects of the Harrah tornadic storm analyzed from dual-Doppler radar data. *Mon. Wea. Rev.*, 106, 233–254.

Jessup, E. A., 1972: Interpretations of chaff trajectories near a severe thunderstorm. *Mon. Wea. Rev.*, 100, 653–661.

Kennedy, P. C., and S. A. Rutledge, 1995: Dual-Doppler and multiparameter radar observations of a bow-echo hailstorm. *Mon. Wea. Rev.*, 123, 921–943.

Klemp, J. B., 1987: Dynamics of tornadic thunderstorms. *Ann. Rev. Fluid Mech.*, 19, 369–402.

Knupp, K. R., and W. R. Cotton, 1982: An intense, quasi-steady thunderstorm over mountainous terrain. Part II: Doppler radar observations of the storm morphological structure. *J. Atmos. Sci.*, 39, 343–358.

Kraus, M. J., 1970: Doppler radar investigation of flow patterns within severe thunderstorms. Preprints, *14th Radar Meteor. Conf.*, Tucson, AZ, Amer. Meteor. Soc., 127–132.

Krauss, T. W., and J. D. Marwitz, 1984: Precipitation processes within an Alberta supercell hailstorm. *J. Atmos. Sci.*, 41, 1025–1034.

Miller, L. J., J. E. Dye, and B. E. Martner, 1983: Dynamical-microphysical evolution of a convective storm in a weakly-sheared environment. Part II: Airflow and precipitation trajectories from Doppler radar observations. *J. Atmos. Sci.*, 40, 2097–2109.

_____, J. D. Tuttle, and G. B. Foote, 1990: Precipitation production in a large Montana hailstorm: Airflow and particle growth trajectories. *J. Atmos. Sci.*, 47, 1619–1646.

NCDC, 1989: *Storm Data*, Vol. 31. [Available from National Climatic Data Center, 151 Patton Avenue, Asheville, NC 28801-5001.]

Orville, R. E., 1991: Lightning ground flash density in the contiguous United States-1989. *Mon. Wea. Rev*, 119, 573–577.

Ramond, D., 1978: Pressure perturbations in deep convection: An experimental study. *J. Atmos. Sci.*, 35, 1704–1711.

Reinking, R. F., and R. J. Meitín, 1993: Vortical circulations within the anvil of a high plains thunderstorm. Preprints, *17th Conf. on Severe Local Storms*, St. Louis, MO, Amer. Meteor. Soc., 242–246.

Rotunno, R., 1981: On the evolution of thunderstorm rotation. *Mon. Wea. Rev.*, 109, 577–586.

_____, and J. B. Klemp, 1982: The influence of the shear-induced pressure gradient on thunderstorm motion. *Mon. Wea. Rev.*, 110, 136–151.

Shmeter, S. M., 1966: Interaction between cumulus clouds and the wind field. *Izv. Acad. Sci. USSR, Atmos. Oceanic Phys.*, 2, 618–621.